Journal of Engineering and Science Research 6 (5): 40-49, 2022
e-ISSN: 2289-7127

DOI: 10.26666/rmp.jesr.2022.5.5

Flow Analysis of Tidal Turbine Array Interaction Using LES

Wan Muhammad Fadhli Arif Wan Zulkafli[a], Anas Abdul Rahman[a], Ayu Abdul-Rahman[b], Azzim Rosli[a], Syafiq Misran[a], Najwa Syafiqa Marzuki[a], Ramadhan Ahmed Ramadhan Bassidiq[a]

[a]Mechanical Engineering Program, Faculty of Mechanical Engineering Technology,
Universiti Malaysia Perlis, Pauh Putra Main Campus, 02600 Perlis, Malaysia.
[b]Department of Mathematics and Statistics, School of Quantitative Sciences,
Universiti Utara Malaysia, 06010 UUM, Sintok, Kedah, Malaysia

Received: 15 August 2022; Revised: 02 September 2022; Accepted: 05 October 2022; Published: 30 October 2022

Abstract: Geographical location of Malaysia is endowed with natural resources such as coal and fossil fuels. Unfortunately, these natural resources will run out shortly if the Malaysian government does not take appropriate measures to conserve them. To ensure that the area has enough energy and sources, a system of utilizing and introducing renewable energy such as solar, rainwater, wave and tidal current energy is established. Vertical axis tidal turbine (VATT) for shallow water applications is the main topic of this study where computational fluid dynamics (CFD) via Large-eddy simulation (LES) and Reynolds-averaged Navier-Stokes (RANS) simulation was performed in investigating the influence of the array interaction of tidal turbines. The VATT is the most suitable tidal turbine in Malaysia because the depth of the water in Malaysia ranges between 20m and 30m. In addition, the hypothetical actuator disk as a representation of the tidal turbine devices, with different turbulence models for simulating tidal turbine wakesinteraction was performed. The tested turbulence models include the k-epsilon, Large Eddy Simulation (LES) and Smagorinsky-Lilly. The evaluation was done by comparing the wake generation between LES and RANS simulations' results against the set of published experimental data regarding various arrays for the tidal turbines. The discussion involves three main parts: (i) pre-processing which concentrates on creating the model and setup parameters, (ii) processing which concentrates on visualizing the simulation data and lastly (iii) post-processing which concentrates on defining the results obtained from the ANSYS software.

Keywords: *Shallow Water, Grid Sensitivity Analysis, Marine Renewable Energy, Turbulence Model, Array Configuration*

1. INTRODUCTION

Malaysia has a coastline of 4,567 kilometres long and is surrounded by the ocean, so there is a great utilization for harnessing energy using waves. Arrays of tidal stream turbines are being developed as systems for generating useful electricity from this large energy resource [1]. Apart from that, tidal energy can be used to replace coal energy, this energy is a renewable energy that is very attractive as an alternative to fossil fuels. It is a renewable resource and highly predictive in its availability [2]. Besides, this tidal energy happens

Corresponding Author: Anas Abdul Rahman, Mechanical Engineering Program, Faculty of Mechanical Engineering Technology, Universiti Malaysia Perlis, Pauh Putra Main Campus, 02600 Arau, Perlis, Malaysia, anasrahman@unimap.edu.my

uniquely and naturally due to the gravitational attraction forces between the earth, sun and moon [3].

The result between the moon and the sun has caused the rise and fall of the sea level twice in one day. The ocean bulged toward the moon due to the attraction forces of the moon acting on the earth. When the sun and the moon are aligned, two tides will occur, namely the spring tide and the neap tide. The spring tide happens when the gravitational forces combine to produce the greatest tidal range. Meanwhile, the neap tide happens when the gravitational forces move the water in a different direction, resulting in lower tidal levels. The research on tidal energy in Malaysia is still currently minimal and there are limited resources on data for the implementation of the tidal turbine in shallow water. Malaysia plans to build tidal turbine energy on the Straits of Malacca because the electric produce is infinite and cannot be depleted [4]. The tidal turbine must be deployed in the field as an array to gather tidal energy efficiently. However, eliminating contacts between upstream turbine wakes and downstream turbine rotors in large turbine arrays may be difficult or impossible, thus tidal array configurations must be constructed to minimize power losses caused by these interactions [5].

The current industrial era has turned into a rapidly evolved world that abundantly on technological advancements and robotics intelligence [6]. In addition, there are increasing societal, economic and institutional pressures to reduce fossil fuels as well as to increase the share of renewable energy and promote the use of renewable energy [7]. SDG 7 is the central hub for promoting sustainable development that ensures energy sustainability, reliability and affordability for all [8]. Many issues are likely to arise at this stage, but the solution with the most sustainable characteristics should be prioritized and implemented [9].

SIMULATION

Modelling

For the current study, the seawater's density is 1023 kg/m^{-3} and the dynamic viscosity is 0.00092 Ns/m^{-2} [10]. In this study, the actuator discs for Horizontal Axis Tidal Turbine (HATT) and Vertical Axis Tidal Turbine (VATT) were chosen because of their quick simulation process as well as simpler meshing process when compared to the other types of numerical modelling. The drawing for the actuator cylinder for both turbines was created using CATIA and SOLIDWORKS before being imported to the ANSYS simulation. There were five steps involved, i.e., geometry, mesh, setup, solution and result. The drawing file was saved using the "*igs*" format which is supported by the ANSYS software.

Apart from that, the domain setup was obtained by doing some literature review to determine the dimension of the domain such as body, faces and edges. To establish the dimensions of the domains and actuator disc, all numerical parameters extracted from the literature review were used. Lastly, the data were compared and validated in their final stages. The study conducted using the first model design is a cylinder via SOLIDWORKS. The parameter values in the design were referred to by Gisrina [11]. Domain dimension, domain parameters as well as the boundary conditions (BC) used are shown in Figure 1 and Table 1.

Meshing is one of the most crucial elements in conducting an accurate simulation. A mesh is made up of elements that contain nodes that represent the geometry's shape. Uneven forms are difficult for a solver to work with, but typical shapes like cubes are much easier. The act of transforming irregular shapes into more recognizable volumes known as "elements" is known as meshing. Besides, meshing mostly takes time to provide simulation results. In this study, the behaviour that was chosen is soft meshing. Table 2 lists the meshing parameters used in this simulation study. Note that all models used in this work are not axis-symmetry, in which the geometry of the domain and object is fully constructed.

Table 1 Domain Parameter Specification

Parameters	Value
Length of Domain	800 m
Width of Domain	80 m
Depth of Domain	30 m
BC Inlet (velocity magnitude)	1 m/s
BC Outlet (pressure)	P_{atm}
BC Wall	No-slip condition

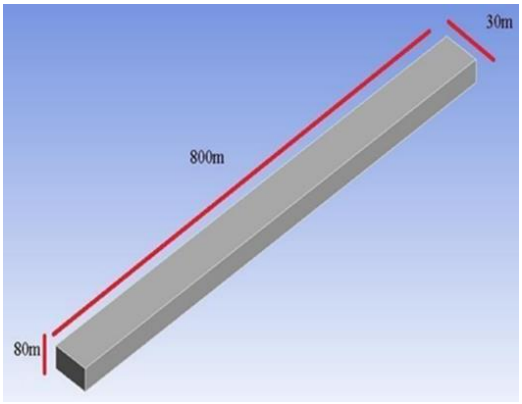

Fig 1 Domain Dimension

Table 2 Meshing Parameter Specification

Parameters	Specification
Method	Tetrahedron
Element Size of the Domain (m)	1.5, 2.0, 2.5, 3.0, 3.5
Element Size of the Surface (m)	0.3
Element Size of the Edge (m)	0.25
Behaviour	Soft

The grid sensitivity is generated by ANSYS Fluent with five different domain element sizes but uses the same parameter values for the faces and edges for each turbulence model. The turbulence model used is LES simulation and the mesh inflating technique was built using the first layer thickness option with 20 maximum layers. Table 3 shows how the element size of the domain decreases from very fine to very coarse where the refinement can increase the number of nodes and elements in the numerical simulation. As shown in Table 3, the time it takes to create a high-quality model affects the simulation's speed. Meshing with a high order of mesh creation takes the longest time to complete. For instance, model using coarse mesh took about 20 minutes for the simulation to complete, while computation time for model with very fine mesh was about 2 hours. All the models were run on a system with the following specification : Intel i5-10300H processor with 16Gb RAM.

Table 3 Grid Sensitivity Analysis

Refinement	Element Size (m)	Nodes	No. of Elements
Very Fine	1.5	827,062	4,677,650
Fine	2.0	358,155	2,001,344
Medium	2.5	191,628	1,054,380
Coarse	3.0	121,385	651,687
Very Coarse	3.5	81,536	434,550

Based on Figure 2, Type 2 (Fine) meshing refinement is the best option for extra numerical calculation and analysis. The mesh size will produce the best results while speeding up numerical computation and analysis compared to finer mesh. The study finds that the maximum velocity produced in numerical solutions is significantly affected by meshing refinement changes from very coarse to very fine, altering the velocity profile at various downstream points. As a result, the optimum alternative for additional numerical calculation and analysis is fine meshing refinement. This mesh size will produce the best results and save time on calculations and analysis when compared to mesh sizes with a finer mesh.

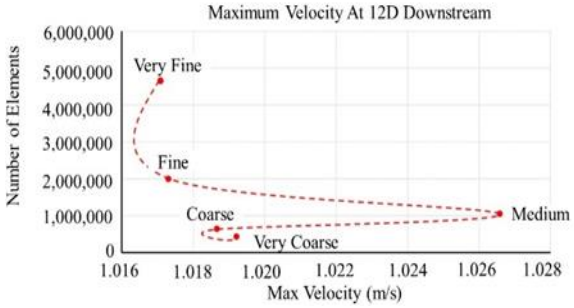

Fig 2 Velocity Profile At 12D Downstream

The pace of the simulation depends on the time required to produce a high-quality model. It has been observed that the process of breaking the continuous geometric space of the domain and faces into smaller shapes to accurately describe the physical shape of the domain, faces and edges, as well as find the numerical solution, takes the longest time. This is followed by medium and coarse meshing. The mesh size influences numerical computation and analysis when compared to a fine mesh.

Table 4 Parameter Specification for Very Fine

Type of Refinement	Element Size (m)	Mesh Generation
(1.5m)	Domain	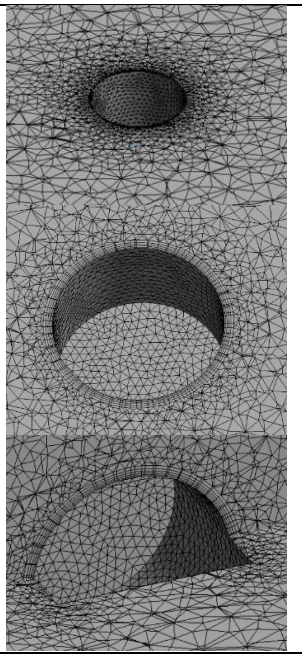
	Faces	
	Edges	

Table 5 Parameter Specification for Fine

Type of Refinement	Element Size (m)	Mesh Generation

(2.0m)	Domain Faces Edges	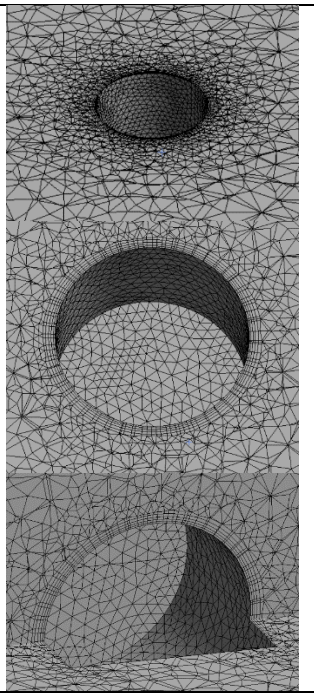

Table 6 Parameter Specification for Medium

Type of Refinement	Element Size (m)	Mesh Generation
(2.5m)	Domain Faces Edges	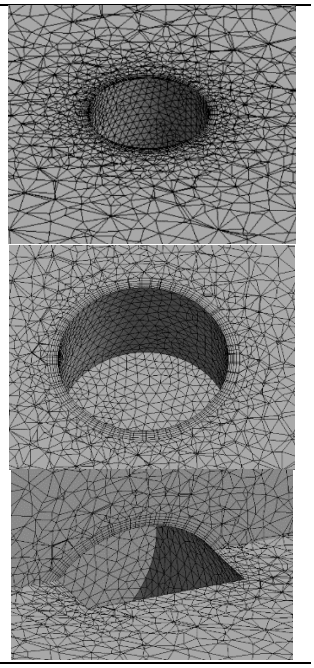

Table 7 Parameter Specification for Coarse

Type of Refinement	Element Size (m)	Mesh Generation
Coarse (3.0m)	Domain Faces Edges	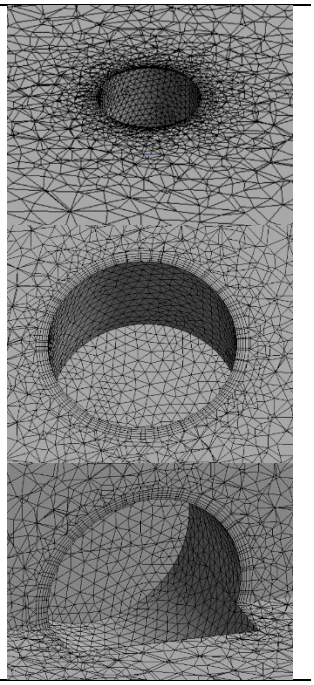

Table 8 Parameter Specification for Very Coarse

Type of Refinement	Element Size (m)	Mesh Generation
(3.5m)	Domain Faces Edges	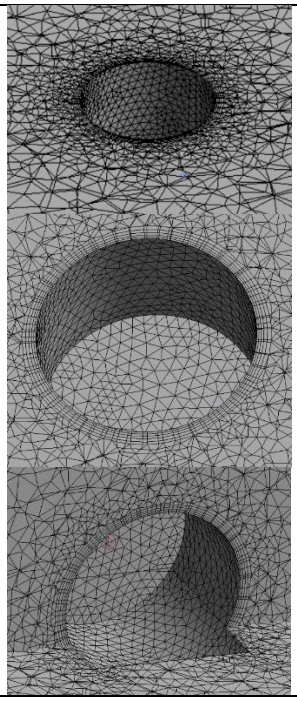

CALCULATION

Tidal Stream Energy Conversion Theory

The kinetic energy of the fluid in a stream tube with a diameter equal to the diameter of the turbine is the maximum power available to a turbine. The density of the medium, the area of the stream tube, A the at the point where it reaches the turbine and the flow velocity, v are all used to calculate this power [12].

$$\rho = \frac{1}{2} A v^3 \quad (1)$$

where ρ is the density of the fluid, A is the area of the turbine rotor and v is the velocity of the fluid.

$$E_{max} = C_p \frac{1}{2} \rho A V^3 \quad (2)$$

where C_p is the power coefficient, ρ is the density of the fluid, A is the area of the turbine rotor and V is the velocity of the fluid.

$$n = \frac{E}{E_{max}} 100 \quad (3)$$

where n is the turbine efficiency, and E is the power output of the turbine.

Reynolds-Averaged Navier Stokes Equation (RANS)

The RANS model is an equation that determines an incompressible fluid's average flow. RANS simulation will take less time to complete than Large-Eddy Simulation (LES). Equation displays the steady-state RANS formulation [13].

$$\rho \frac{\partial \overline{u_i}}{\partial t} + \rho \overline{u_j} \frac{\partial \overline{u_i}}{\partial x_j} = -\frac{\partial \bar{p}}{\partial x_i} + \frac{\partial}{\partial x_j} (\mu \frac{\overline{u_i}}{\partial x_j} - \rho \overline{u_i' u_j'}) \quad (4)$$

where $\bar{p}$ is time-averaged relative pressure, $-\rho \overline{u_i' u_j'}$ is the Reynolds stress tensor, ρ is the liquid density, and μ is the liquid's dynamic viscosity.

RESULT AND DISCUSSION

Comparison Results between RANS and LES Simulation

The study focuses on the velocity contour developed across the domain. The velocity of contour has been used to identify the wake that is formed and the characteristic of the wake such as near and far wake can be observed as well. The wake generated can show whether the domain's wake recovery is fast or slow from upstream to downstream. The wake generated may show how quickly or slowly the domain recovers from the upstream to the downstream wake. The results are shown for the velocity contour for single cylinder, single-row inline and staggered array. The velocity of the tidal current is 0.56m/s – 1m/s based on Omar Yaakob's research [13].

Comparison Results between RANS and LES Simulation for Single Cylinder

Figure 5 and Figure 6 illustrate the velocity contour from two different simulations. In Figure 5, the domain of the velocity is depicted by a yellow colour region with a value of 1.13 m/s. It shows a reduction in the velocity value after passing through the turbine.

In Figure 6, there is only one cylinder in the simulation and the highest velocity contour range is 1.55 m/s. The velocity after passing through the cylinder seems to be biased based on the LES simulation.

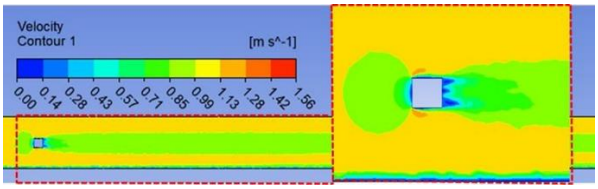

Fig 5 Velocity Contour for Single Cylinder using RANS

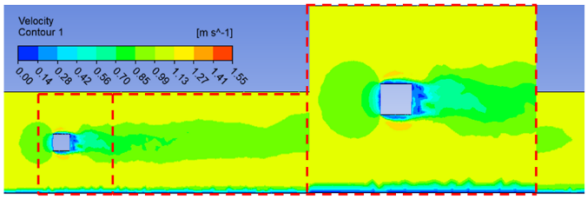

Fig 6 Velocity Contour for Single Cylinder using LES

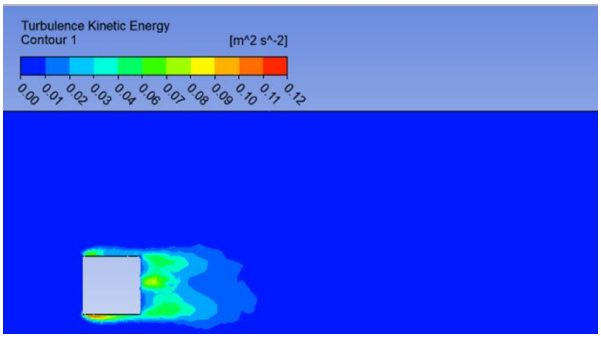

Fig 7 Turbulent Kinetic Energy for Single Cylinder

In the top view, the turbulence kinetic energy that passes through the turbine slowly fades away from 0.03 m/s to 0.00m/s. In Figure 7, there is one tiny region in yellow colour (0.09m/s) and one tiny region in high turbulence kinetic energy illustrated by the red colour (12 m/s). The low-turbulence kinetic energy happens after passing

through the cylinder and later, increases to 0.03m/s (the light blue indicates the value of the velocity).

Figure 8 illustrated the velocity magnitude using two different simulations, namely RANS and LES at different distances set at 6D, 8D and 12D. The pointer is shown in the figure experimental data ("x"), RANS (Blue Circle) and LES (Purple Triangle). The experimental data were extracted from Clary et al [14]. The plotting for the LES at 12D downstream seems to be different from the 6D and 8D downstream. This is caused by the distance between the hypothetical actuator cylinder.

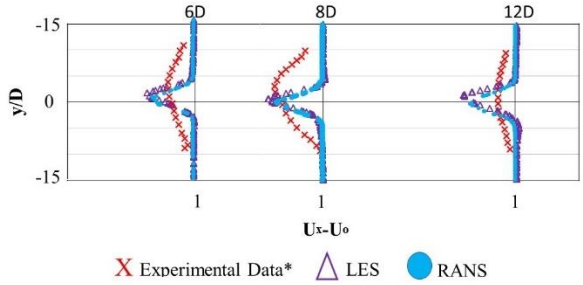

Fig 8 Comparison Experimental Data Between RANS and LES Simulation at 6D, 8D and 12D Downstream

Comparison Results between RANS and LES Simulation for Single-Row Inline

In Figure 9, the velocity contour passing through the turbines is in the triangle pattern and finally back to its initial velocity. It shows that the velocity is connected between the turbines. The highest velocity between the turbines appears because the inlet velocity did not strike any of the turbines.

Figure 10 shows the single-row inline turbine and the velocity contour that was captured using the LES simulation. The fluid flow after passing through the turbine is like the wave pattern the red region colour that values 1.42 m/s to 1.74 m/s is in between the turbines which did not strike any turbines.

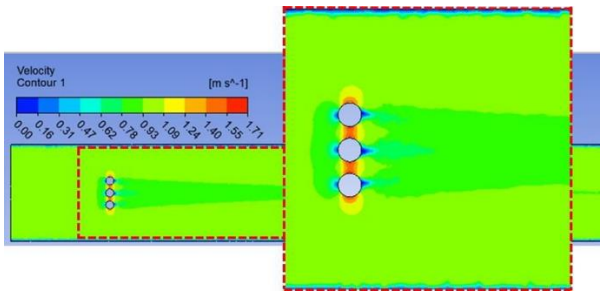

Fig 9 Velocity Contour for Single-Row Inline using RANS

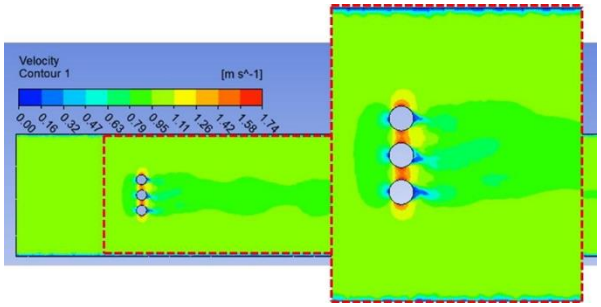

Fig 10 Velocity Contour for Single-Row Inline using LES

Based on Figure 11, the turbulence kinetic energy of the fluid is approaching the centre. The maximum turbulent kinetic energy in this RANS simulation is 0.08m/s with a short area of red colour behind the turbines. The flow of the turbulent kinetic energy approaches the centre suggests that the energy is starting to reform to the original energy.

A comparison analysis was developed against numerical data extracted from Stallard et al [15] in assessing the appropriateness of concluding the arrangement on the single-row inline. From Figure 12, the comparison between the RANS and LES simulations via the numerical and experimental data were illustrated in different shapes at 8D downstream. The peak velocity for the RANS simulation is 1.01005 and as for the LES simulation, it is 1.01777. The trend for LES simulation seems to recover earlier than the RANS simulation.

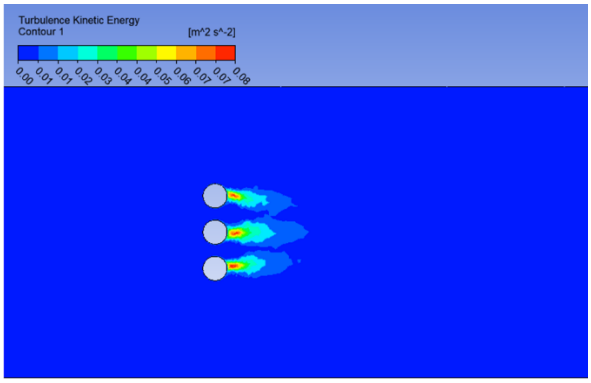

Fig 11 Turbulent Kinetic Energy for Single-Row Inline

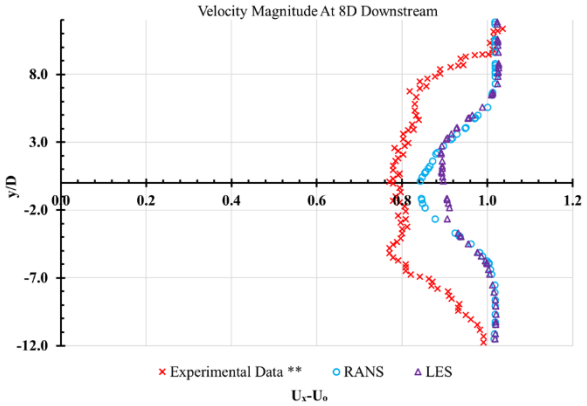

Fig 12 Velocity Magnitude At 8D Downstream

In Figure 13, the plotted experimental data between RANS and LES almost overlap. The plots indicate minor differences between the performance of the RANS and LENS. The trend for the LES simulation at 8D Downstream is identical to the RANS simulation when compared using the experimental data. The maximum velocity point for the RANS is 1.01884m/s and for the LES is 1.03m/s.

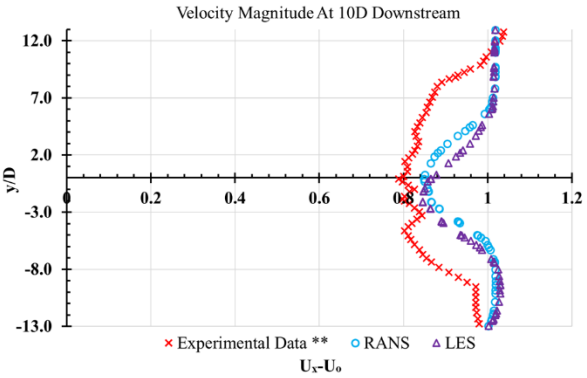

Fig 13 Velocity Magnitude At 10D Downstream

The comparison between experimental data and the RANS and LES is illustrated in Figure 14 via different shapes where for the RANS, it is a circle and for the LES, is it a triangle. The plotting shown in Figure 14 is at 12D downstream. The trend for both simulation RANS and LES seems to merge. This is because the data capture for this 12D downstream used different turbulence models. The turbulence model for RANS is k-epsilon and for the LES is Smagorinsky-Lilly. To highlight, k-epsilon model is a robust two-transport-equation model that is commonly used to characterise turbulent flow conditions. On the other hand, Smagorinsky-Lilly model is suitable for applications with high Reynolds number to ensure proper energy dissipation.

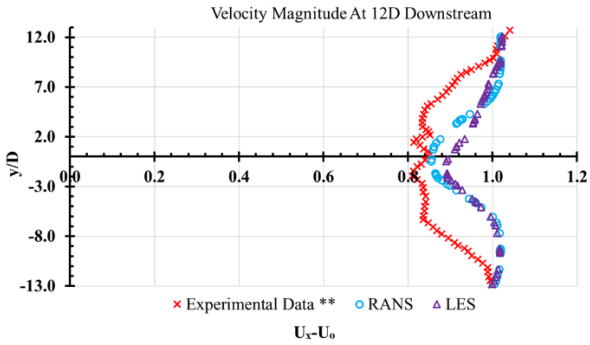

Fig 14 Velocity Magnitude At 12D Downstream

Turbulent Intensity Plotting For 8D,10D and 12D

A comparison of the turbulence strength between experimental data from Stallard et al [15] and numerical data of the single row-inline is done to determine the suitability of finalizing the arrangement. At each cross-section, the turbulent flow's intensity is nearly constant regardless of the water depth. It is well known that the turbulence strength of the entering turbulent tidal has an impact on the power generation of tidal turbines.

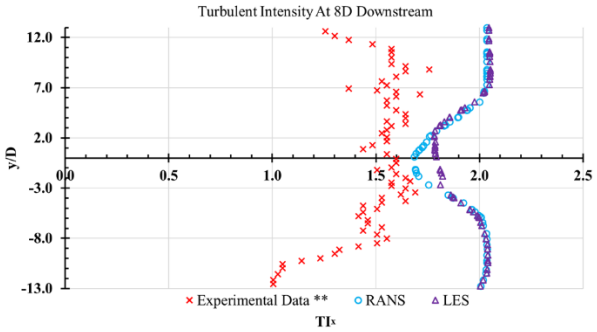

Fig 15 Turbulent Intensity At 8D Downstream

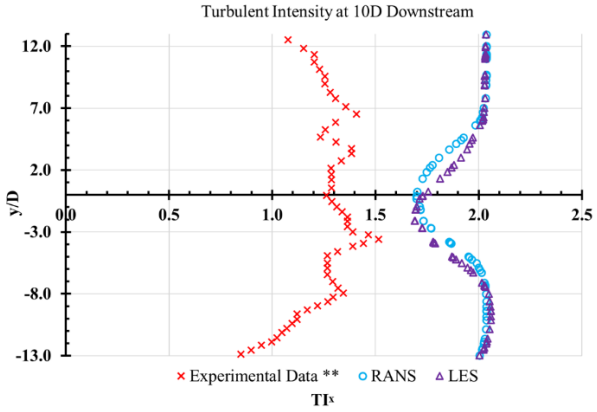

Fig 16 Turbulent Intensity At 10D Downstream

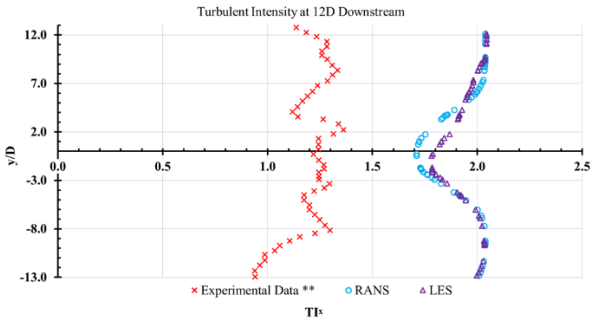

Fig 17 Turbulent Intensity At 12D Downstream

Mean Absolute Errors of Single-Row Inline

Absolute errors are one of the many methods that refer to the magnitude of difference between a prediction and the actual value of an observation. The errors of points were taken for each plot. The following formula defines the mean absolute error concerning the average of all absolute errors.

Table 9 Mean Absolute Errors for Single Row-Inline

Comparison of Absolute Errors	Mean Absolute Errors %	
Velocity Magnitude	8D RANS	9.87
	8D LES	9.02
	10D RANS	7.55
	10D LES	7.83
	12D RANS	6.18
	12D LES	6.94
Turbulent Intensity	8D RANS	44.03
	8D LES	45.10
	10D RANS	63.33
	10D LES	63.65
	12D RANS	68.36
	12D LES	69.63

Comparison Results between RANS and LES Simulation for Staggered Array

In Figure 18, the simulation was conducted using the RANS simulation with a total of 7 turbines. The longitudinal spacing of the turbine is 1.5D and the lateral spacing of 0.3D. The turbine models are arranged in staggered arrays where they had an identical fluid flow pattern with a higher velocity before passing through the turbine and a lower velocity after passing through the turbines. Most of the turbines had slow-moving flow after passing through the turbines but in the third turbine, the slow-moving flow region seems to happen after the velocity strikes the turbine. The heavy blue colour indicates more energy loss as the velocity strikes the third turbine.

Figure 19 shows the velocity contour using the LES simulation with the aforementioned staggered array. For the far wake generation, the velocity contour after passing through the turbine is likely to fade away. The patterns for the velocity contour in each turbine are not the same, it happens in various situations. There are some velocities in a low state and there are also some with a small region of light green colour with the value is 0.95 m/s, in this LES simulation, the flow pattern of the velocity mostly strikes most of the turbines and slow-moving flow starts to appear behind the turbines. Each of the slow-moving flows behind the turbine shows different patterns. This is because LES simulation uses the transient state.

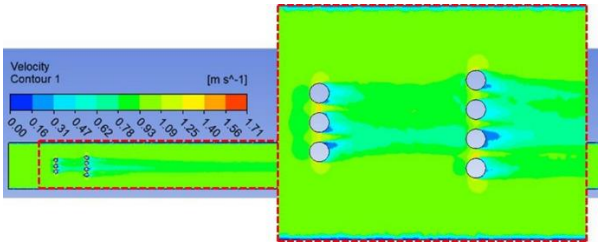

Fig 18 Velocity Contour for Staggered Array using RANS

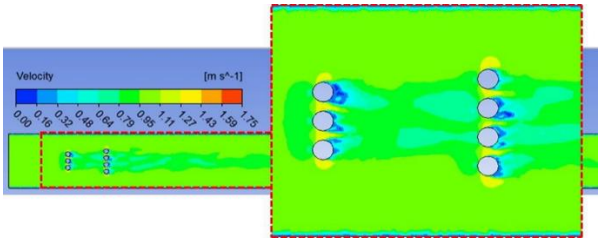

Fig 19 Velocity Contour for Staggered Array using LES

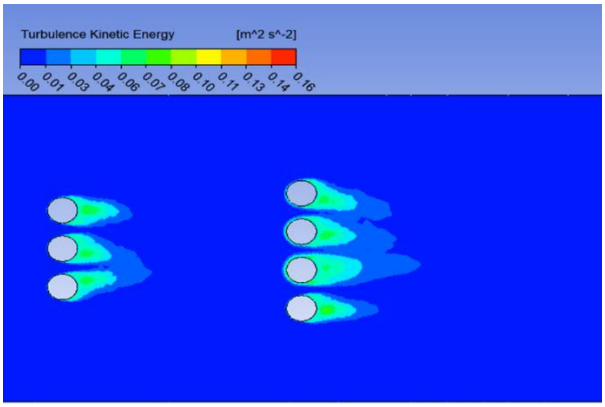

Fig 20 Velocity Contour for Staggered Array using LES

Figure 20 shows the turbulent kinetic energy that passes through all the turbines. Most of the turbulent kinetic energy has the same pattern after striking the turbine and likely behind the turbines had the region light blue colour with a value of 0.04 m/s. There is no high

turbulence kinetic energy for staggered arrays. For the staggered arrays, the flow of the turbulence kinetic energy seems to approach the centre after passing through the turbines and finally, resorts to the original energy.

Figure 21 shows the comparison of velocity in staggered array arrangement with a spacing of 1.5D for lateral spacing and 8D for longitudinal spacing. The experimental data is extracted from Olczak et al [16]. As depicted in the figure, the findings of the RANS and LES simulation were compared against the experimental data. For the RANS plotting, the plotting shape seems identical to the experimental data but for the LES simulation, it is not. The highest velocity of RANS simulation is 1.04529 m/s and the highest velocity point for LES simulation is 1.05057 m/s.

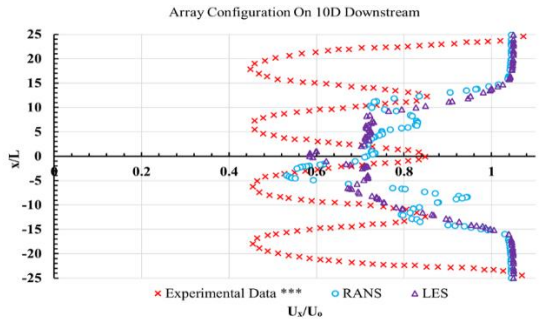

Fig 21 Array Configuration On 10D Downstream

Figure 22 shows the comparison between RANS and LES with experimental data at 12D downstream. The pattern plotting for the RANS and LES at 12D downstream is almost the same as the experimental data. As for velocity at 12D downstream, the LES plotting start to follow the experimental data trend at the coordinates (1.0333,14.0515). Comparing the trend between the RANS and LES, the LES trend is far more similar to the experimental data than the RANS. Additionally, Table 10 summarises the comparison of mean absolute errors for staggered array configuration between the two tested models.

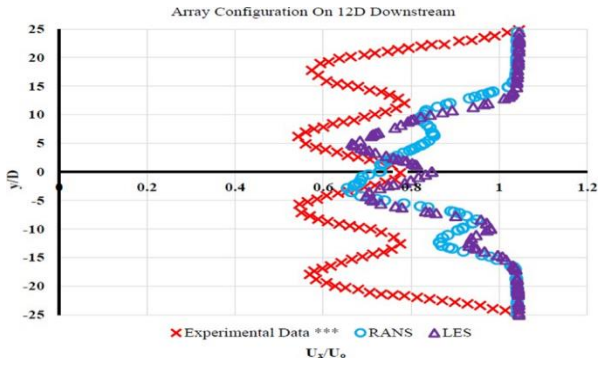

Fig 22 Array Configuration On 12D Downstream

Table 10 Mean Absolute Errors for Staggered Array

Comparison of Absolute Errors	Mean Absolute Errors %	
Velocity Magnitude	10D RANS	22.95
	10D LES	23.87
	12D RANS	20.54
	12D LES	21.41

CONCLUSION

Comparing the results between RANS and LES bring various data and differences for each array interaction, the single cylinder, single-row inline and staggered array. First, the differences can be seen through the results from velocity contours for each simulation. The results from the velocity contour show the different patterns of the velocity contour that pass-through turbines using two different simulations. Moreover, the mean absolute errors highlight the percentage differences between the velocity downstream and turbulence intensity by capturing the data from various distances, i.e., 8D,10D and 12D. The mean absolute errors show a significant difference which is almost a 50% gap. The mean absolute error for the staggered array for 10D RANS is 22.95% and for 10D LES is 23.87%. Hence it can be concluded that the significant difference for both simulations is only about 0.92%.

ACKNOWLEDGEMENTS

The authors gratefully acknowledge the support received from the Ministry of Higher Education Malaysia through the Fundamental Research Grant Scheme for Research Acculturation of Early Career Researchers (FRGSRACER) RACER / 1 / 2019 / TK07 / UNIMAP/1. Additionally, the authors are also thankful for the support received from Universiti Malaysia Perlis, specifically from the Research Management Centre (RMC).

.

REFERENCES

[1] I. Afgan, J. McNaughton, S. Rolfo, D. D. Apsley, T. Stallard, and P. Stansby, "Turbulent flow and loading on a tidal stream turbine by LES and RANS," *Int. J. Heat Fluid Flow*, vol. 43, pp. 96–108, Oct. 2013, doi: 10.1016/j.ijheatfluidflow.2013.03.010.

[2] S. Nash and A. Phoenix, "A review of the current understanding of the hydro-environmental impacts

of energy removal by tidal turbines," *Renewable and Sustainable Energy Reviews*, vol. 80. Elsevier Ltd, pp. 648–662, 2017, doi: 10.1016/j.rser.2017.05.289.

[3] H. Faez Hassan, A. El-Shafie, and O. A. Karim, "Tidal current turbines glance at the past and look into future prospects in Malaysia," *Renewable and Sustainable Energy Reviews*, vol. 16, no. 8. pp. 5707–5717, Oct. 2012, doi: 10.1016/j.rser.2012.06.016.

[4] A. S. Sakmani, W. H. Lam, R. Hashim, and H. Y. Chong, "Site selection for tidal turbine installation in the Strait of Malacca," *Renewable and Sustainable Energy Reviews*, vol. 21. Elsevier Ltd, pp. 590–602, 2013, doi: 10.1016/j.rser.2012.12.050.

[5] F. Attene, F. Balduzzi, A. Bianchini, and M. Sergio Campobasso, "Using experimentally validated navier-stokes cfd to minimize tidal stream turbine power losses due to wake/turbine interactions," *Sustain.*, vol. 12, no. 21, pp. 2–26, Nov. 2020, doi: 10.3390/su12218768.

[6] N. M. Suki, N. M. Suki, A. Sharif, S. Afshan, and K. Jermsittiparsert, "The role of technology innovation and renewable energy in reducing environmental degradation in Malaysia: A step towards sustainable environment," *Renew. Energy*, vol. 182, pp. 245–253, Jan. 2022, doi: 10.1016/j.renene.2021.10.007.

[7] F. S. Mohd Chachuli, N. Ahmad Ludin, M. A. Md Jedi, and N. H. Hamid, "Transition of renewable energy policies in Malaysia: Benchmarking with data envelopment analysis," *Renew. Sustain. Energy Rev.*, vol. 150, Oct. 2021, doi: 10.1016/j.rser.2021.111456.

[8] R. Madurai Elavarasan *et al.*, "Envisioning the UN Sustainable Development Goals (SDGs) through the lens of energy sustainability (SDG 7) in the post-COVID-19 world," *Appl. Energy*, vol. 292, Jun. 2021, doi: 10.1016/j.apenergy.2021.116665.

[9] Y. Li and Y. Niu, "A commentary on 'The socio-economic implications of the coronavirus pandemic (COVID-19): A review,'" *International Journal of Surgery*, vol. 95. Elsevier Ltd, Nov. 01, 2021, doi: 10.1016/j.ijsu.2021.106048.

[10] A. Roberts, B. Thomas, P. Sewell, Z. Khan, S. Balmain, and J. Gillman, "Current tidal power technologies and their suitability for applications in coastal and marine areas," *J. Ocean Eng. Mar. Energy*, vol. 2, no. 2, pp. 227–245, May 2016, doi: 10.1007/s40722-016-0044-8.

[11] I. Between and T. Turbine, "Jurnal Teknologi INTERACTION BETWEEN TIDAL TURBINE WAKES : CASE STUDY OF SHALLOW WATER APPLICATION," vol. 1, pp. 1–5, 2020.

[12] T. P. Lloyd, S. R. Turnock, and V. F. Humphrey, "Assessing the influence of inflow turbulence on noise and performance of a tidal turbine using large eddy simulations," *Renew. Energy*, vol. 71, pp. 742–754, 2014, doi: 10.1016/j.renene.2014.06.011.

[13] B. Daniel and J. Nicklas, "The Development of a Vertical Axis Tidal Current Turbine," *KTH Ind. Eng. Manag.*, p. 84, 2013, [Online]. Available: http://www.diva-portal.org/smash/record.jsf?pid=diva2:537660&dswid=6120.

[14] V. Clary, T. Oudart, P. Larroudé, J. Sommeria, and T. Maître, "An optimally-controlled RANS Actuator force model for efficient computations of tidal turbine arrays," *Ocean Eng.*, vol. 212, Sep. 2020, doi: 10.1016/j.oceaneng.2020.107677.

[15] T. Stallard, R. Collings, T. Feng, and J. Whelan, "Interactions between tidal turbine wakes: Experimental study of a group of three-bladed rotors," *Philos. Trans. R. Soc. A Math. Phys. Eng. Sci.*, vol. 371, no. 1985, Feb. 2013, doi: 10.1098/rsta.2012.0159.

[16] A. Olczak, T. Stallard, T. Feng, and P. K. Stansby, "Comparison of a RANS blade element model for tidal turbine arrays with laboratory scale measurements of wake velocity and rotor thrust," *J. Fluids Struct.*, vol. 64, pp. 87–106, Jul. 2016, doi: 10.1016/j.jfluidstructs.2016.04.001.